Available online at www.sciencedirect.com
ScienceDirect
Journal of Solid State Chemistry 179 (2006) 3568–3574
JOURNAL OF SOLID STATE CHEMISTRY
www.elsevier.com/locate/jssc

The nature of the orthorhombic to tetragonal phase transition in $Sr_{1-x}Ca_xMnO_3$

Qingdi Zhou, Brendan J. Kennedy*

School of Chemistry, The University of Sydney, Sydney, NSW 2006, Australia

Received 15 May 2006; received in revised form 2 July 2006; accepted 18 July 2006
Available online 29 July 2006

Abstract

The orthorhombic–tetragonal phase transition in the perovskite series $Sr_{1-x}Ca_xMnO_3$ $0.4 \leqslant x \leqslant 0.6$ has been studied by synchrotron X-ray powder diffraction. At room temperature the Ca rich oxides $x \geqslant 0.45$ have the orthorhombic *Pbnm* superstructure whereas $Sr_{0.6}Ca_{0.4}MnO_3$ is two phases with both tetragonal *I*4/*mcm* and orthorhombic *Pbnm*. Analysis of the octahedral tilts suggest the co-existence of these two phases is a consequence of a first-order *I*4/*mcm* to *Pbnm* transition. The evolution of the structure of $Sr_{0.5}Ca_{0.5}MnO_3$ with temperature is also described and this is found to evolve from orthorhombic to tetragonal and ultimately cubic.

Keywords: Oxides; X-ray diffraction; Crystal structure; Phase transition; Perovskite

1. Introduction

The rich array of physical, electronic and magnetic properties displayed by perovskite-type oxides has stimulated numerous studies aimed at establishing structure-property relationships [1]. Perovskite-type oxides are used as capacitors, ferroelectrics, non-linear optics and piezoelectrics. Perovskite manganites also display colossal magnetoresistance as a consequence of competing magnetic properties and charge and orbital ordering [2,3]. Given the pervasiveness of perovskites in the solid state it is hardly surprising that a large body of structural information exists for such oxides [1,4].

Chmaissem et al. [5] recently showed that the antiferromagnetic transition temperature, T_N, in the series $Sr_{1-x}Ca_xMnO_3$ was sensitive to the effective size of the A-type cation and the average Mn–O–Mn bond angles, regardless of the structural symmetry. These workers concluded that for Sr rich oxides $x<0.3$ the structure was cubic $Pm\bar{3}m$ ($a^0\ a^0\ a^0$), tetragonal *I*4/*mcm* ($a^0\ a^0\ a^-$) for $0.3<x<0.4$ and orthorhombic *Pbnm* ($a^+\ b^-\ b^-$) for $x>0.4$. The progressive lowering of symmetry upon addition of Ca is a consequence of the introduction of cooperative in-phase (+) and out-of-phase (−) tilts of the MnO_6 octahedra in response to the progressive decrease in the effective size of the A-type cation [6,7]. This size effect is often quantified for ABO_3 perovskites by the tolerance factor *t*,

$$t = \frac{R_A + R_O}{\sqrt{2}(R_B + R_O)},$$

where R_A and R_B are the ionic sizes of the A- and B-types cations and R_O the radii of the oxide anion.

The influence of the effective size of the A-type cation (or more accurately the ratio of the relative sizes of the A and B-type cations) on the structures and phase transitions in ABO_3 perovskites, where A is an alkaline earth cation (Ca, Sr or Ba) and B, a tetra-valent metal, has now been studied for a number of systems [5,8–15]. Oxides where the B-site cation is a second or third row transition metal or late *P*-block element such as Sn have been found to display the sequence of phases:

$$Pnma(a^+\ b^-\ b^-) \overset{\text{continuous}}{\longrightarrow} Imma(a^0\ b^-\ b^-) \overset{\text{firstorder}}{\longrightarrow} I4/mcm(a^0\ a^0\ c^-) \overset{\text{continuous}}{\longrightarrow} Pm\bar{3}m(a^0\ a^0\ a^0).$$

The first-order nature of the *Imma*−*I*4/*mcm* transition can result in co-existence of these two phases. For the

*Corresponding author. Fax: +61 2 9351 3329.
E-mail address: kennedyb@chem.usyd.edu.au (B.J. Kennedy).

0022-4596/$ - see front matter © 2006 Elsevier Inc. All rights reserved.
doi:10.1016/j.jssc.2006.07.039

continuous transitions the two phases will not co-exist near the transition point. The $Sr_{1-x}Ca_xTiO_3$ system has been extensively studied [16–21] and early reports [8] of a *Cmcm* phase have now been shown to be incorrect [16]. Rather the weight of evidence suggests the sequence to be:

$$Pnma(a^+\ b^-\ b^-) \rightarrow Pbcm \rightarrow I4/mcm(a^0\ a^0\ c^-) \rightarrow Pm\bar{3}m(a^0\ a^0\ a^0).$$

Ranson et al. [16] have suggested that the $I4/mcm$ phase is in fact orthorhombic in *Imma* and that there is a first order *Imma*–$Pm\bar{3}m$transition in this series although this suggestion has not been widely accepted. The *Pbcm* phase exists as a consequence of both tilting of the octahedra and cation displacement. Much less is known about the structures of the other first row transition metal oxides but for V and Mn the available data [5,22] indicates the sequence is

$$Pnma(a^+\ b^-\ b^-) \overset{\text{first order}}{\longrightarrow} I4/mcm\ (a^0\ a^0\ c^-) \overset{\text{continuous}}{\longrightarrow} Pm\bar{3}m\ (a^0\ a^0\ a^0),$$

there being no suggestion for the existence of the *Imma* phase observed for the 4d and 5d oxides. It should be stressed that the experimental evidence to verify this is poor and an *Imma* phase has been observed in some mixed valence $Ln_{1-x}A_xMnO_3$ and $Gd_{1-x}Sr_xFeO_3$ perovskites [23,24]. Similarly more complex behaviour is observed for other Fe and Co perovskites as a consequence of valence state variations [25,26]. The absence of the *Pbcm* phase in the V and Mn oxides implicates a second order Jahn–Teller effect for the Ti series, although this suggestion has not been explored in detail.

The current evidence outlined above suggests that there may be a difference in the behaviour of the ABO_3 perovskites depending on the nature of the B-type cation with the lighter elements displaying a different sequence of phases than when B is a heavier element. If proven, this hypothesis has implications for our understanding of the properties of the perovskite form of $MgSiO_3$ that exists in the earth's core [27]. In order to establish the presence or absence of the *Imma* phase in the $AMnO_3$ oxides we have investigated the structure of a number of such oxides around the orthorhombic-tetragonal phase boundary using synchrotron X-ray powder diffraction. Variable temperature studies were also undertaken for one representative example in the series $Sr_{1-x}Ca_xMnO_3$.

2. Experimental

2.1. Syntheses

The crystalline samples of $Sr_{1-x}Ca_xMnO_3$ ($x = 0.4$, 0.45, 0.5, 0.55, 0.6) were prepared by the solid-state reaction of stoichiometric quantities of $CaCO_3$ (99.95%, Aldrich), $SrCO_3$ (99.9%, Aldrich), and MnO_2 (99.999%, Aithacu Chemical Corp.) using a muffle furnace operating in air. The preparation of the two Ca rich oxides $x = 0.55$ and 0.60 proved straightforward, however as the Sr content was increased the maximum reaction temperature had to be carefully controlled to avoid formation of the hexagonal phase. The use of lower reaction temperatures required longer than usual annealing times. The heating procedures are given in Table 1, and were developed to produce highly crystalline single-phase samples.

2.2. Conventional X-ray diffraction

The samples were initially examined by powder X-ray diffraction measurements using Cu-Kα radiation ($\lambda = 1.5406$ Å) on a Shimadzu D-6000 Diffractometer (40 kV, 30 mA, divergence and anti-scatter slits 1 mm, receiver and detector slits 0.3 mm, respectively). These measurements did not reveal any impurity phases.

2.3. Electron microscopy

Samples were examined either as powders or as sintered pellets produced by applying 9–10 ton pressure onto a 10 mm disc. The discs were then heated at 1150 °C for 12 h. The samples were mounted on aluminum sample holders and then carbon coated to minimize charging effects. The scanning electron micrograph (SEM) and accompanying energy–dispersive X-ray (EDX) analysis were carried out using a Phillips XL 30 scanning electron microscope, with a tungsten filament operating at 25 kV, and a working distant of 11 mm. The EDX analysis of elemental composition, was performed in conjunction with the imaging process using an EDAX model XL-30 operated under the DX-4eDX ZAF operating system (Version 3.3). Analysis was performed with scan times averaging 90 s.

Table 1
Heating Schedule employed for the samples $Sr_{1-x}Ca_xMnO_3$

	800 °C	900 °C	1000 °C	1150 °C	1230 °C	1250 °C	1260 °C	1280 °C	1300 °C
$Sr_{0.6}Ca_{0.4}MnO_3$[a]	18 h				70 h		200 h	105 h	
$Sr_{0.55}Ca_{0.45}MnO_3$[a]	18 h				70 h		200 h	20 h	
$Sr_{0.5}Ca_{0.5}MnO_3$[a]	18 h				70 h		200 h		
$Sr_{0.45}Ca_{0.55}MnO_3$	12 h	24 h	72 h	128 h		40 h			20 h
$Sr_{0.4}Ca_{0.6}MnO_3$	12 h	24 h	72 h	128 h		40 h			20 h

[a]The samples were quenched after each heating procedure.

2.4. Synchrotron XRD

Room and variable temperature synchrotron X-ray powder diffraction patterns were collected on a high resolution Debye Scherrer diffractometer at beamline 20B, the Australian National Beamline Facility, Photon Factory, Japan [28]. The samples were finely ground and loaded into 0.3-mm capillaries that were rotated during the measurements. Data were recorded at a wavelength of 0.80123 Å using up to three BAS2000 Fuji image plates as detectors. Each image plate is 20×40 cm and each covers 40° in 2θ, allowing data to be collected over the range $2\theta = 5$–125° with a step size of 0.01005°. A thin strip ca. 0.5-cm wide is used to record each diffraction pattern. Variable temperature data were collected, using a custom-built furnace, at temperatures of up to 800 °C, for these measurements data was collected over the range $2\theta = 5$–85°. All measurements were performed under vacuum to minimize air scatter. Structural parameters were refined by the Rietveld method using the program RIETICA [29]. A pseudo-Voigt function was used to model the peaks. The background was estimated by linear interpolation between regions where there were no Bragg peaks.

3. Results and discussion

3.1. Room temperature structures

Based on the earlier study of Chmaissem et al. [5] we focused the present study at compositions near $x = 0.5$, that is near the *Pbnm*–*I*4/*mcm* phase transition. The synchrotron diffraction patterns for the four samples of $Sr_xCa_{1-x}MnO_3$ ($x = 0.6$, 0.55, 0.5, 0.45) were well fitted in the orthorhombic structure of space group *Pbnm* [30]. A representative example for $x = 0.5$ is shown in Fig. 1. The refined lattice parameters and atomic coordinates for these were in excellent agreement with the results reported by Chmaissem et al. [5] for the two common samples ($x = 0.5$ and 0.6). A key feature of the present work is the exceptional signal-to-noise afforded by the synchrotron diffractometer that allows for clear identification of the reflections associated with the tilting of the MnO_6 octahedra. This is highlighted in the inset of Fig. 1. The appropriate space group for these oxides was established by considering the observed metric and the extinction of these superlattice reflections. For $x = 0.5$ the 0 2 1 reflection near $2\theta = 18.5°$ is assigned as an *X*-point reflection arising from a combination of in-phase tilting of the MnO_6 octahedra and displacement of the A-type cation. The 210/120 pair near $2\theta = 19.5°$ are *M*-point reflections associated with in-phase tilting and the 211/103/121 peaks near $2\theta = 20.5°$ are *R*-point reflections from out-of-phase tilts. The presence of all these reflections and the cell metric demonstrates the structure to be in *Pbnm* ($a^+ b^- b^-$).

As the Sr content was progressively increased in the series $Sr_{1-x}Ca_xMnO_3$ from $x = 0.6$ to 0.4 the intensity of the *M*-point reflections such as the 210/120 pair near $2\theta = 19.5°$ decreased noticeably, but critically did not totally vanish (see Fig. 2). However attempts to fit the pattern for $x = 0.4$ in *Pbnm* were unsuccessful with $R_p \sim 17.8\%$ and $R_{wp} \sim 23.1\%$. The pattern for this composition appeared tetragonal as reported by Chmaissem et al. [5] and could be better fitted in *I*4/*mcm* giving $R_p \sim 9.8\%$ and $R_{wp} \sim 12.7\%$, although this model failed to fit the weak *M*-point reflections (that are forbidden in *I*4/*mcm*). These reflections could be fitted in an alternate tetragonal model *P*4/*mbm* ($a^0 a^0 c^+$) however *P*4/*mbm* does not allow for the observed *R*-point reflections and the *R*-factors remained unacceptably high $R_p \sim 11.9\%$ and $R_{wp} \sim 15.5\%$. Ultimately the pattern was fitted using a mixture of orthorhombic *Pbnm* and tetragonal *I*4/*mcm*, the final *R*-factors being

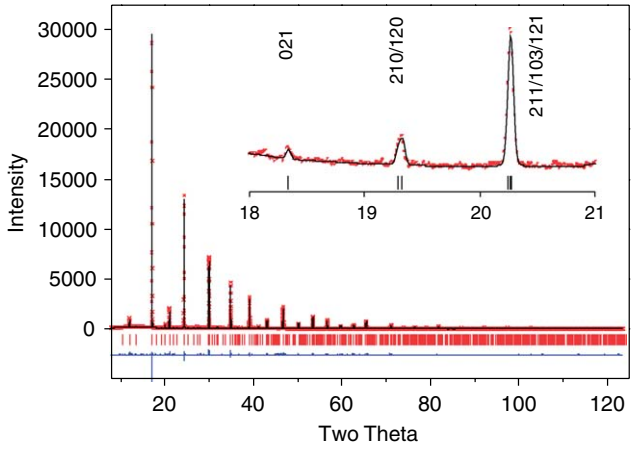

Fig. 1. Best-fit Rietveld refinement using synchrotron powder diffraction data for $Sr_{0.5}Ca_{0.5}MnO_3$ at room temperature. The inset shows selected superlattice reflections associated with the tilting of the MnO_6 octahedra.

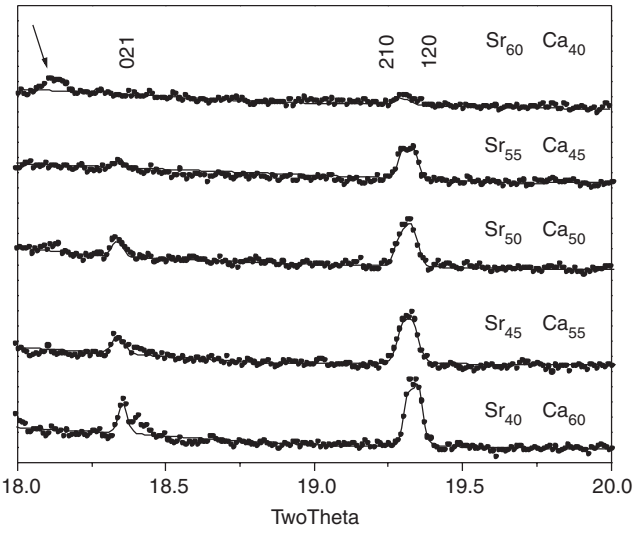

Fig. 2. Portions of the synchrotron powder diffraction patterns for $Sr_{1-x}Ca_xMnO_3$ samples showing the *X*-point (0 2 1) and *M*-point (2 1 0/1 2 0) reflections indicative of in-phase tilting of the MnO_6 octahedra. The arrowed feature in the top profile is from an unidentified impurity. The intensity of these reflections is ca. 0.2% that of the strongest reflection.

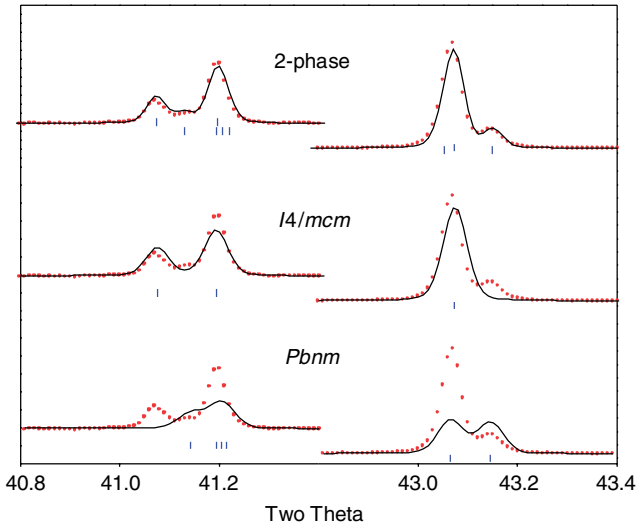

Fig. 3. Portions of the synchrotron powder diffraction pattern for $Sr_{0.6}Ca_{0.4}MnO_3$ ($x = 0.4$) illustrating the coexistence of the two-phases *Pbnm* and *I4/mcm*. The Rietveld refinement shows the sample contains 30(1)% orthorhombic phase.

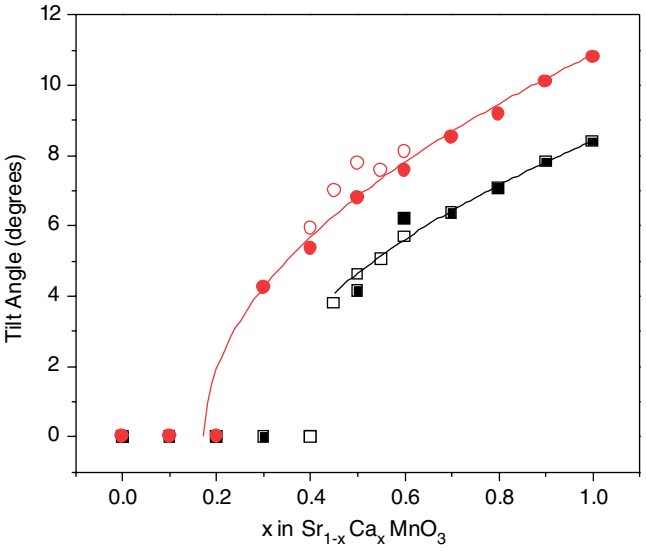

Fig. 4. Variation of the in-phase and out-of-phase tilts in the series $Sr_{1-x}Ca_xMnO_3$. The open symbols are the present results and the closed symbols from Ref. [5]. The solid lines are fits to an expression of the type $\varphi^2 = Ax + C$.

4.57% and 6.39%, Fig. 3. This two-phase model accounted for both the *R*- and *M*-point reflections. The co-existence of the *Pbnm* and *I4/mcm* phases is consistent with Howard and Stokes [7] group theoretical analysis that demonstrated any transition between these must be first order. Equally importantly co-existence of *Pbnm* and *I4/mcm* phases is strong evidence for the absence of an intermediate *Imma* phase. By analogy with the $AZrO_3$ and $AHfO_3$ (A = Ba/Sr) [9–11] oxides the *Imma* phase is expected to form continuously from *Pbnm* as t is reduced and the *Imma* phase directly transforms to a *I4/mcm* phase with a small two-phase region. No attempt was made to establish if a single phase $x = 0.5$ sample could be obtained at room temperature, presumably careful annealing of the sample just below the *Pbnm–Imma* transition temperature could achieve this.

The observed c/a ratio further indicates that the tetragonal phase is in *I4/mcm* and is not a metrically tetragonal variant of the *Imma* phase. Assuming approximately rigid octahedra the out-of-phase tilting about the *c*-axis in *I4/mcm* is expected to result in an increase in c and consequent reduction in the size of the *ab* plane resulting in the c/a ratio (of the pseudocubic cell) being greater than 1. For *Imma* the out-of-phase tilting is about the diad axis parallel to the *b*-axis and will led to an expansion in the *ab* plane and consequent reduction in the *c*-axis. That is, for *Imma* c/a should be less than 1. The refined lattice parameters for the tetragonal phase in $Sr_{0.6}Ca_{0.4}MnO_3$ are $a = 5.33963(2)$ and $c = 7.58089(3)$ Å giving, after scaling to the primitive equivalent values $a_p = a_t/2^{0.5}$ and $c_p = c_t/2$, $c/a = 1.004$.

It is generally accepted that the replacement of Sr by Ca in $Sr_{1-x}Ca_xMnO_3$ drives the orthorhombic distortion due to a reduction in t as calculated from tabulated ionic radii [30] from 1.001 in $SrTiO_3$ to 0.970 in $CaTiO_3$. Likewise for $Ba_{1-x}Sr_xZrO_3$, $BaZrO_3$ has $t = 1.004$ and is cubic while $SrZrO_3$ has $t = 0.953$ and is orthorhombic at room temperature [9,12]. While the tolerance factor decreases as the Sr is replaced by Ca in $Sr_{1-x}Ca_xMnO_3$ it is interesting to note that t for $CaMnO_3$ is 1.008 and for $SrMnO_3$ it is 1.041. If size alone was important, then $CaMnO_3$ would be expected to be cubic, since $t \sim 1.00$, whereas it is found to be orthorhombic [5,31]. We speculate

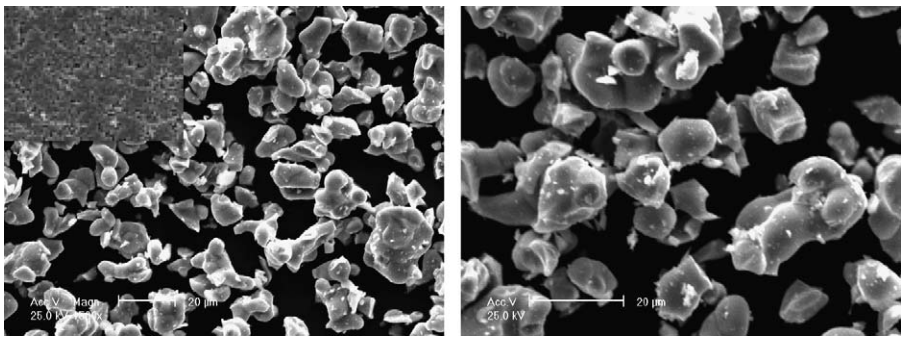

Fig. 5. SEM images of powdered samples $Sr_{0.5}Ca_{0.5}MnO_3$ (left) and $Sr_{0.6}Ca_{0.4}MnO_3$ (right), the inserted image in the left was taken from the same sample in the form of a sintered pallet.

that this subtle difference in behavior is related to the partial occupancy of the 3-d orbitals in the manganites.

The magnitude of the tilts in the orthorhombic *Pbnm* phase can be estimated from the refined structural parameters of the O(2) anions at $1/4-u$, $1/4+v$, w, where the out-of-phase tilt is given by $\tan\psi = 2(u+v)$ and the in-phase tilts by $\tan\varphi = 4\sqrt{2}w$. The composition dependence of the tilts obtained here, and calculated from the published work of Chmaissem et al. [5] for the series $Sr_{1-x}Ca_xMnO_3$ are illustrated in Fig. 4. Two things are notable from this figure; firstly there is good agreement between our results and those of Chmaissem et al. [5]. This is somewhat remarkable given the differences in the preparative conditions used [32] and the different sensitivities of the two diffraction probes, X-rays and neutrons, used. We have noted previously the excellent signal-to-noise possible with the synchrotron diffractometer used in this study and this coupled with the large number of resolved reflections measured over a wide *d*-range ($5^\circ \leqslant 2\theta \leqslant 125^\circ$ at 0.80123 Å) corresponds to 9.2 Å $\leqslant d \leqslant$ 0.45 Å) allows us to refine accurate and precise atomic coordinates for these types of oxides. Secondly the composition dependence of the in-phase and out-of-phase tilts were well fitted by an expression of the type $\phi^2 = Ax + C$ where A and C are constants and x the composition, Fig. 4. From this fitting the critical compositions of $x = 0.183$ and 0.280 were estimated for the removal of the out-of-phase and in-phase tilts, respectively. The former value is in reasonable agreement with the observed behavior, however the latter significantly overestimates the observed critical composition. The bulk of the sample with $x = 0.4$, $Sr_{0.6}Ca_{0.4}MnO_3$, is clearly tetragonal in *I*4/*mcm* as consequence of the loss of the in-phase tilts. Experimentally, we observe the in-phase tilts to abruptly vanish near $x = 0.4$. This is consistent with a first-order phase transition and is inconsistent with a continuous *Pbnm–Imma* transition that would occur by the progressive loss of the in-phase tilts around a diad axis ($a^0\ b^-\ b^-$).

3.2. Electron microscopy

In order to verify that the two-phases observed in $Sr_{0.6}Ca_{0.4}MnO_3$ was not a consequence of sample inhomogeneity, this and the other samples were subjected to extensive X-ray microanalysis using a combination of scanning electron microscopy and EDX microanalysis. The SEM images showed all the samples were similar and there was no evidence from back-scattering images for any inhomogeneity. As illustrated in Fig. 5 we failed to observe any features in the SEM images that could be associated with non-uniform Sr:Ca distribution. Likewise the EDX analysis at up to nine different areas of the sample invariably gave Sr:Ca:Mn ratios in excellent agreement with the expected values, Table 2. In brief we found no evidence from the analytical microscopy for any phase separation. Finally, we note that a diffraction pattern of $Sr_{0.6}Ca_{0.4}MnO_3$ recorded at 300 °C was well fitted in

Table 2
EDX molar ratios of chemical compositions vs the theoretical values

Samples	Elemental molar ratio (calc.) Sr:Ca:Mn	Elemental molar ratio (expe.) Sr:Ca:Mn
$Sr_{0.6}Ca_{0.4}MnO_3$	1:0.7:1.7	1:0.7:1.6
$Sr_{0.55}Ca_{0.45}MnO_3$	1:0.8:1.8	1:0.9:1.8
$Sr_{0.5}Ca_{0.5}MnO_3$	1:1:2.0	1:1.1:1.9
$Sr_{0.45}Ca_{0.55}MnO_3$	1:1.2:2.2	1:1.2:2.0
$Sr_{0.4}Ca_{0.6}MnO_3$	1:1.5:2.5	1:1.4:2.2

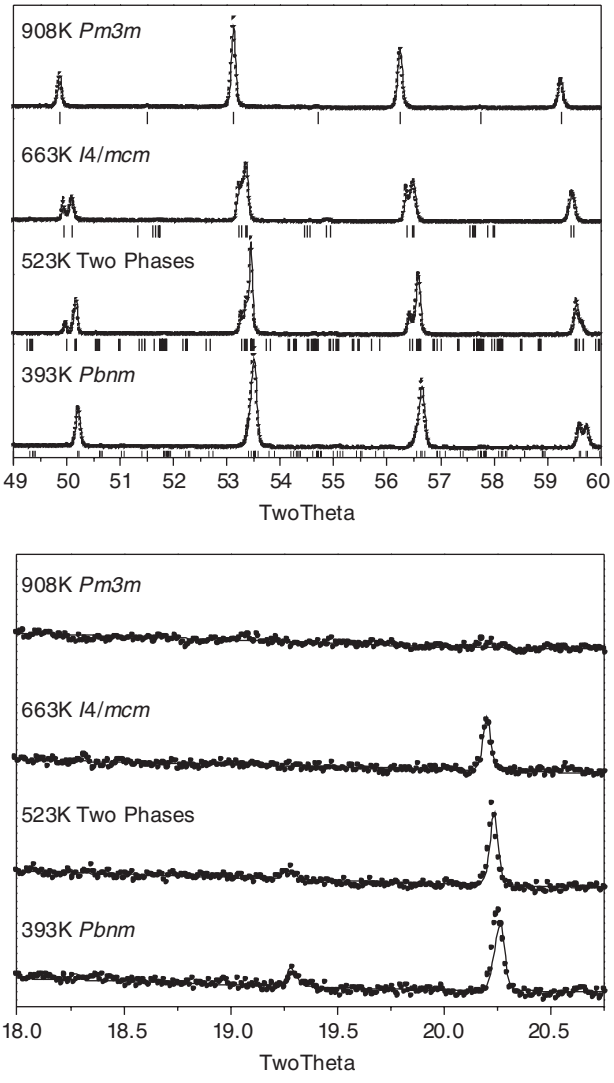

Fig. 6. Portions of the diffraction patterns for $Sr_{0.5}Ca_{0.5}MnO_3$ highlighting the changes in the diffraction patterns as a function of temperature. The lower angle region shows the changes in the diagnostic superlattice reflections and the higher angle region better illustrates the change in the cell metric. The *M*-point reflections indicative of in-phase tilts (near $2\theta = 19.4^\circ$) are observed to 523 K. On this scale the X-point reflection (near $2\theta = 18.4^\circ$) is not discernable. The *R*-point reflections (near $2\theta = 20.3^\circ$), indicative of out-of-phase tilts, persist to 838 K. Above this temperature the structure is cubic. The Rietveld refinement shows the sample to contain 45(1)% orthorhombic phase at 523 K. The results of the refinements for these patterns are listed in Table 3.

$I4/mcm$ with $a = 5.35842(4)$ and $c = 7.59270(7)$ Å, $c/a = 1.002$, there being no evidence for any X- or M-point reflections in the pattern at this temperature. The widths of the diffraction peaks at this temperature were similar to those observed in all the other samples studied here and are not indicative of a range of compositions.

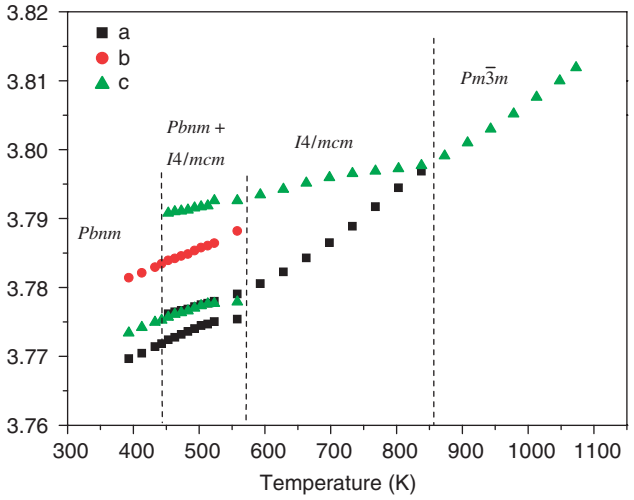

Fig. 7. The temperature dependence of the lattice parameters for $Sr_{0.5}Ca_{0.5}MnO_3$.

3.3. Variable temperature diffraction studies

The structure of $Sr_{0.5}Ca_{0.5}MnO_3$ was investigated over the temperature range 298–1073 K. As noted above the structure was orthorhombic in $Pbnm$ at room temperature and the patterns recorded at or below 433 K were well fitted by this choice of space group (Fig. 6). At higher temperatures it was necessary to include a second $I4/mcm$ phase in the refinements and this two-phase ($I4/mcm + Pbnm$) model proved adequate for patterns recorded between 443 and 523 K. Above this satisfactory fits could be obtained using a single phase $I4/mcm$ ($558 < T < 838$ K) or $Pm\bar{3}m$ ($838 < T < 1073$ K) model. These results are summarized in Fig. 7 and representative refined structural parameters are given in Table 3. As is evident from Fig. 7 in both the two-phase region and in the single-phase tetragonal region the c/a ratio is greater than 1.00 indicative of $I4/mcm$.

The nature of the tetragonal to cubic phase transition was investigated by examination of the spontaneous tetragonal strains calculated from the lattice parameters as $\varepsilon_t = (c_t - \sqrt{2}a_t)/\sqrt{3}a_o$ [33] where a_t and c_t are the

Table 3
Refined structural parameters obtained from synchrotron X-ray diffraction data for $Sr_{0.5}Ca_{0.5}MnO_3$ at selected temperatures

Temperature (K)	393	523		663	908
Space group	*Pbnm*	Mixed two phases		*I4/mcm*	*Pm3̄m*
		Pbnm	*I4/mcm*		
Ca (Sr)					
x	−0.0010(8)	0.002(2)	0	0	0.5
y	0.5002(4)	0.4991(8)	0.5	0.5	0.5
z	0.25	0.25	0.25	0.25	0.5
B_{iso}	1.27(2)	1.50(4)	1.36(4)	1.73(3)	1.99(3)
Mn					
x	0	0	0	0	0
y	0	0	0	0	0
z	0	0	0	0	0
B_{iso}	0.79(2)	0.76(4)	0.80(4)	0.97(2)	1.15(2)
O_1					
x	−0.032(2)	0.031(4)	0	0	0.5
y	0.028(1)	−0.025(3)	0	0	0
z	0.25	0.25	0.25	0.25	0
B_{iso}	0.9(2)	1.3(4)	1.8(1)	1.6(1)	3.10(5)
O_2					
x	0.235(2)	0.228(2)	0.277(1)	0.2733(6)	
y	0.270(1)	0.269(2)	0.777(1)	0.7733(6)	
z	0.022(1)	−0.019(2)	0	0	
B_{iso}	2.0(1)	1.4(2)	1.9(1)	2.7(1)	
a (Å)	5.3311(1)	5.3387(1)	5.3429(1)	5.3518(1)	3.8010(1)
b (Å)	5.3477(1)	5.3548(1)			
c (Å)	7.5468(1)	7.5554(1)	7.5840(1)	7.5903(1)	
R_p	4.57	3.97		5.28	4.81
R_{wp}	5.75	5.14		7.04	6.43

observed tetragonal lattice parameters and a_o is the equivalent (strain free) cubic lattice parameters estimated by extrapolation from the cubic region. A plot of ε_t^2 against temperature was linear indicating the transition is continuous and tricritical in nature. The magnitude of the tilts in the tetragonal phase was estimated from the refined atomic coordinates and this showed a similar (φ^2) temperature dependence.

A feature of these variable temperature results is the extensive two-phase (*Pbnm* and *I*4/*mcm*) region. Again we note that this is indicative of a first-order phase transition and is not expected to occur for a continuous phase transition. This is taken as strong evidence against the involvement of an intermediate *Imma* phase in the transition.

4. Conclusion

The structures of the perovskites $Sr_{1-x}Ca_xMnO_3$ $0.4 \leqslant x \leqslant 0.6$ were investigated as a function of composition and temperature using synchrotron X-ray powder diffraction. For $x \geqslant 0.45$ the materials all adopted an orthorhombic structure in *Pbnm* at room temperature. The diffraction pattern for $Sr_{0.6}Ca_{0.4}MnO_3$ showed the presence of two phases, tetragonal in *I*4/*mcm* and orthorhombic in *Pbnm*. Heating this to 573 K yielded a single-phase (*I*4/*mcm*) structure. This behavior is indicative of a first-order *Pbnm* to *I*4/*mcm* transition. Variable temperature structural studies of $Sr_{0.5}Ca_{0.5}MnO_3$ show a similar first order *Pbnm* to *I*4/*mcm* transition with extensive two-phase region. Above 573 K the sample is tetragonal (*I*4/*mcm*) and this undergoes a continuous transition to cubic near 850 K. We find no evidence for a intermediate *Imma* phase and suggesting the behavior of the first row transition metal perovskites AMO_3 is different than the analogous heavier second and third row oxides such as $SrZrO_3$ or $SrRuO_3$.

Acknowledgments

The authors gratefully acknowledge the support of this work from the Australia Research Council. Synchrotron diffraction measurements were performed at the Australian National Beamline Facility with support from the Australian Synchrotron Research Program, which is funded by the Commonwealth of Australia under the Major National Research Facilities Program. The authors also gratefully acknowledge Dr. James Hester for assistance at ANBF.

References

[1] R.H. Mitchell, Perovskites: Modern and Ancient, Almaz Press, Ontario, Canada, 2002.
[2] A.P. Ramirez, J. Phys. C Conden. Matter 9 (1997) 8171.
[3] J.B. Goodenough, Phys. Rev. 164 (1967) 785.
[4] P.M. Woodward, Acta Crystallogr. B: Struct. Crystallogr. Cryst. Chem. B 53 (1997) 32.
[5] O. Chmaissem, B. Dabrowski, S. Kolesnik, J. Mais, D.E. Brown, R. Kruk, P. Prior, B. Pyles, J.D. Jorgensen, Phys. Rev. B 64 (2001) 134412.
[6] A.M. Glazer, Acta Crystallogr. B: Struct. Crystallogr. Cryst. Chem. B 28 (1972) 3384.
[7] C.J. Howard, H.T. Stokes, Acta Crystallogr. B: Struct. Crystallogr. Cryst. Chem. B 54 (1998) 782.
[8] C.J. Ball, B.D. Begg, D.J. Cookson, G.J. Thorogood, E.R. Vance, J. Solid State Chem. 139 (1998) 238.
[9] B.J. Kennedy, C.J. Howard, G.J. Thorogood, J.R. Hester, J. Solid State Chem. 161 (2001) 106.
[10] L. Li, B.J. Kennedy, Y. Kubota, K. Kato, R.F. Garrett, J. Mater. Chem. 14 (2004) 263.
[11] E.H. Mountstevens, J.P. Attfield, S.A.T. Redfern, J. Phys. C Conden. Matter 15 (2003) 8315.
[12] C.J. Howard, K.S. Knight, B.J. Kennedy, E.H. Kisi, J. Phys. C Conden. Matter 12 (2000) L677.
[13] B.J. Kennedy, B.A. Hunter, J.R. Hester, Phys. Rev. B 65 (2002) 224103.
[14] B.J. Kennedy, C.L. Howard, B.C. Chakoumakos, Phys. Rev. B 60 (1999) 2972.
[15] M. Glerup, K.S. Knight, F.W. Poulsen, Mater. Res. Bull. 40 (2005) 507.
[16] P. Ranson, R. Ouillon, J.P. Pinan-Lucarre, P. Pruzan, S.K. Mishra, R. Ranjan, D. Pandey, J. Raman Spec. 36 (2005) 898.
[17] S.K. Mishra, R. Ranjan, D. Pandey, P. Ranson, R. Ouillon, J.P. Pinan-Lucarre, P. Pruzan, J. Solid State Chem. 178 (2005) 2846.
[18] S. Qin, A.I. Becerro, F. Seifert, J. Gottsmann, J. Jiang, J. Mater Chem. 10 (2000) 1609.
[19] C.J. Howard, R.L. Withers, B.J. Kennedy, J. Solid State Chem. 160 (2001) 8.
[20] R. Ranjan, D. Pandey, W. Schuddinck, O. Richard, P. De Meulenaere, J. Van Landuyt, G. Van Tendeloo, J. Solid State Chem. 162 (2001) 20.
[21] B.J. Kennedy, C.J. Howard, B.C. Chakoumakos, J. Phys. C Conden. Matter 11 (1999) 1479.
[22] J. Garcia-Jaca, J.L. Mesa, M. Insausti, J.I.R. Larramendi, M.I. Arriortua, T. Rojo, Mater. Res. Bull. 34 (1999) 289.
[23] P.M. Woodward, T. Vogt, D.E. Cox, A. Arulraj, C.N.R. Rao, P. Karen, A.K. Cheetham, Chem. Mater. 10 (1998) 3652.
[24] J. Blasco, J. Stankiewicz, J. Garcia, J. Solid State Chem. 179 (2006) 898.
[25] M. James, K.S. Wallwork, R.L. Withers, D.J. Goossens, K.F. Wilson, J. Horvat, X.L. Wang, M. Colella, Mater. Res. Bull. 40 (2005) 1415.
[26] M. Schmidt, M. Hofmann, S.J. Campbell, J. Phys. C Conden. Matter 15 (2003) 8691.
[27] L.-G. Liu, Geophys. Res. Lett. 1 (1974) 277.
[28] T.M. Sabine, B.J. Kennedy, R.F. Garrett, G.J. Foran, D.J. Cookson, J. Appl. Crystallogr. 28 (1995) 513.
[29] C.J. Howard, B.A. Hunter, A Computer Program for Rietveld Analysis of X-ray and Neutron Powder Diffraction Patterns, Lucas Heights Research Laboratories, NSW, Australia, 2000, pp. 1–27.
[30] R.D. Shannon, Acta Crystallogr. A 32 (1976) 751.
[31] Q. Zhou, B.J. Kennedy, J. Phys. Chem. Solids 67 (2006) 1595.
[32] J. Topfer, U. Pippardt, I. Vogt, R. Kriegel, Solid State Sci. 6 (2004) 647.
[33] M.A. Carpenter, A.I. Becerro, F. Seifert, Am. Mineral. 86 (2001) 348.